YALE PEABODY MUSEUM

JOURNAL OF MARINE RESEARCH

The *Journal of Marine Research,* one of the oldest journals in American marine science, published important peer-reviewed original research on a broad array of topics in physical, biological, and chemical oceanography vital to the academic oceanographic community in the long and rich tradition of the Sears Foundation for Marine Research at Yale University.

An archive of all issues from 1937 to 2021 (Volume 1–79) are available through EliScholar, a digital platform for scholarly publishing provided by Yale University Library at https://elischolar.library.yale.edu/.

Requests for permission to clear rights for use of this content should be directed to the authors, their estates, or other representatives. The *Journal of Marine Research* has no contact information beyond the affiliations listed in the published articles. We ask that you provide attribution to the *Journal of Marine Research.*

Yale University provides access to these materials for educational and research purposes only. Copyright or other proprietary rights to content contained in this document may be held by individuals or entities other than, or in addition to, Yale University. You are solely responsible for determining the ownership of the copyright, and for obtaining permission for your intended use. Yale University makes no warranty that your distribution, reproduction, or other use of these materials will not infringe the rights of third parties.

Glider measurements of overturning in a Kelvin-Helmholtz billow train

by W. D. Smyth[1,2] and S. A. Thorpe[1]

ABSTRACT

The prospects for glider-based measurement of turbulence statistics are assessed using direct numerical simulation data representing breaking Kelvin-Helmholtz (KH) billows in a stratified, parallel shear flow. Transects tilted upstream against the shear tend to produce overestimates of overturning; those tilted with the shear produce underestimates. Low-angle transects can produce illusory overturning as the braid between the KH billows is crossed. Statistical features of the bias in displacement scales are related to geometrical aspects of KH billows. Results are interpreted in the context of a hypothetical effort to characterize overturning in a strongly sheared current (e.g. the Equatorial Undercurrent) using nonvertical profiles.

1. Introduction

Ocean mixing events typically begin with the overturning of isopycnals. The resulting potential energy is then converted to kinetic energy at the scale of the overturn and subsequently cascaded to the dissipative scales. The vertical scale of overturns is readily estimated using vertical profilers (Gregg, 1987) and can be used to infer other turbulence statistics of interest (e.g. Dillon, 1982; 1984; Wijesekera and Dillon, 1997; Smyth *et al.*, 2001). The prospects for measuring overturning have improved with the development of autonomous gliders (Eriksen, 2009), which can collect data more economically than locally-attended profilers. The price of this efficiency is that gliders do not normally profile vertically, and may therefore suffer bias in the estimation of the vertical overturn scale. The same applies to towed vehicles such as Marlin (Moum *et al.*, 2002) and Seasoar. The companion paper (Thorpe, 2012; hereafter T12) uses simple geometrical models to predict this bias in various classes of flows where overturning may occur. In internal waves, a profile taken at a low angle can register overturning even when none is present; the profile slope need only be within the range of isopycnal slopes generated by the wave. In turbulent eddies, the computed bias is a few tens of percent or less. While significant, this is not large compared with the factor-of-two uncertainty that is normally assumed in shear probe measurements and need therefore not be a barrier to glider measurements of overturning.

1. School of Ocean Sciences, University of Bangor, Menai Bridge, Bangor, LL58 8PH, United Kingdom.
2. Permanent address: College of Oceanic and Atmospheric Sciences, Oregon State University, Corvallis, Oregon, 97331, U.S.A. ***email: smyth@coas.oregonstate.edu***

Here, we extend T12 by running virtual "gliders" through simulated flow fields, computing the resulting density profiles and displacement scales, and comparing with the results from vertical profiles. The dataset comes from a direct numerical simulation (DNS) of turbulence resulting from the breaking of a train of Kelvin-Helmholtz (KH) billows. (The internal wave breaking problem of T12 is not considered here.) KH billows are an important class of mixing processes in the ocean, due largely to their ubiquity at the the edges of near-surface and boundary currents and their role in the turbulent breakdown of internal waves (e.g., Woods, 1968; Thorpe, 1978, 1987; Gregg, 1987; Geyer and Smith, 1987; Seim and Gregg, 1994; Smyth *et al.*, 2001; Li and Yamazacki, 2001; Moum *et al.*, 2003; Van Haren and Gostiaux, 2009; Moum *et al.*, 2011; Smyth *et al.*, 2011). While the essential instability was understood many decades ago (e.g., Taylor, 1931), the mechanics of the transition to turbulence are a subject of ongoing research (Baines and Mitsudera, 1994; Thorpe and Holt, 1995; Geyer *et al.*, 2010) as are the mechanisms governing the spatial extents of a billow patch (Thorpe, 2002; Smyth, 2004). The spatial distribution of billow patches in the ocean is largely unknown. The capacity to profile turbulent shear flows from various directions (Eriksen, 2009, T12) promises important new insights into these questions, and it is to this end that the present theoretical investigation is directed.

In Section 2, the DNS methodology is described and an overview given of the resulting simulated mixing event. Also described is the method of computing displacement scales based on a sampling of trajectories at given angles. A bias function Bf is defined as the ratio of the displacement scale computed at a given angle to that computed from vertical profiles through the same event at the same time. Results are given in Section 3. We compute Bf directly from the DNS data over the duration of the mixing event and for a range of trajectory angles. The main features of Bf are identified and compared with the elliptical vortex model. Aspects of Bf that differ from the theoretical model are explained in terms of the geometrical properties of the KH billows and the resulting sheared, stratified turbulence. Implications for the measurement of the displacement scale using both vertical profilers and gliders are discussed in Section 4, and the conclusions are summarized in Section 5.

2. Methods and overview

a. Direct simulations

The simulated mixing event employed here is a numerical solution of the inhomogeneous Navier-Stokes equations in the Boussinesq approximation. The numerical code is based on Winters *et al.* (2004), using a refined grid for the density field as described by Smyth *et al.* (2005). The kinematic viscosity ν is 1.0×10^{-6} m^2 s^{-1} and the diffusivity κ is 1.4×10^{-7} m^2 s^{-1} (so that the Prandtl number ν/κ is 7) consistent with thermally-stratified water. Boundary conditions are periodic in the streamwise x and cross-stream y directions, and free-slip and insulating in the vertically upward direction z. Domain dimensions are $L_x = 4.19$ m, $L_y = 0.87$ m and $L_z = 2.18$ m. The array size is $772 \times 160 \times 400$ for density, $386 \times 80 \times 200$ for all other fields.
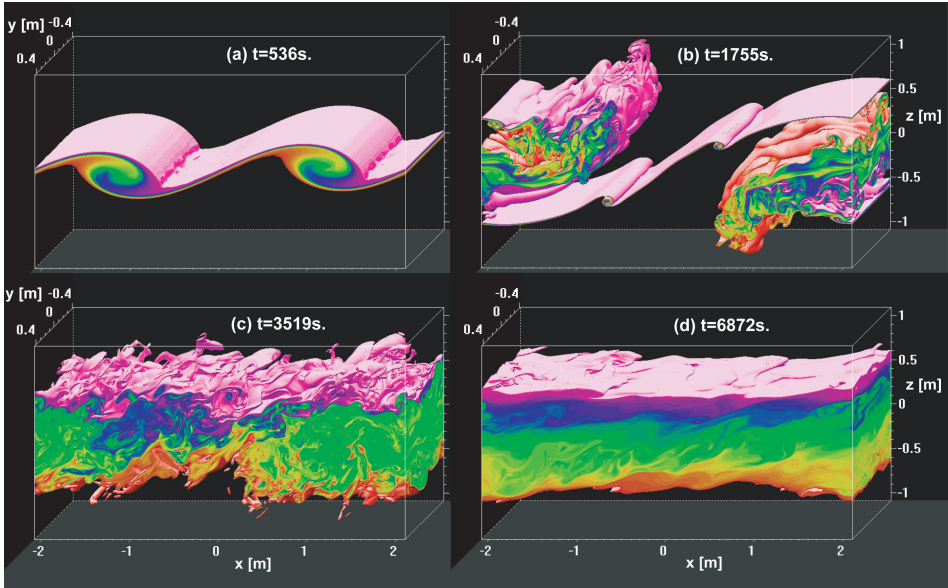
Figure 1. Density field at $t = 536s$ (a), $t = 1755s$ (b), $t = 3519s$ (c) and $t = 6872s$ (d). Colors range from $\rho_0 - 0.6\Delta\rho$ (purple) to $\rho_0 + 0.6\Delta\rho$ (red); values outside this range are rendered transparent.

Initial mean profiles of streamwise velocity and density are chosen to represent a stratified, parallel shear layer:

$$\frac{u(z)}{\Delta u} = -\frac{\rho(z) - \rho_0}{\Delta\rho} = \tanh\left(\frac{z}{h}\right) \qquad (1)$$

with half-changes $\Delta\rho = 1.6 \times 10^{-3}$ kg m^{-3} in density and $\Delta u = 5.3 \times 10^{-3}$ m s^{-1} in streamwise velocity, mean density 1027 kg m^{-3}, and half-thickness $h = 0.15$ m. A small perturbation is added to excite primary and secondary instabilities as described in Smyth *et al.* (2005). The initial Richardson number $gh\rho_0^{-1}\Delta\rho\Delta u^{-2}$ is 0.08, within the range in which pairing is observed. The initial Reynolds number $h\Delta u\nu^{-1}$ is 800. *Re* is limited by computational hardware; the present value is small compared to most ocean mixing events, but is an advance beyond previous studies (e.g., Smyth *et al.*, 2001; Inoue and Smyth, 2009).

The domain accommodates two wavelengths of the primary Kelvin-Helmholtz instability which grow to large amplitude (Fig. 1a), then pair and break (Fig. 1b). Secondary Kelvin-Helmholtz rollers (e.g. Smyth, 2003) are visible on the braids during pairing (Fig. 1b). After breaking, the flow attains a turbulent state (Fig. 1c) which decays (Fig. 1d) over about an hour, leaving a stable parallel shear layer. The simulation is terminated when disturbances reach the upper and lower boundaries of the computational domain.

For most of the broad range of stratified shear flows that have been studied via lab experiments and *in situ* observations, detailed visualizations such as Figure 1 are not available.
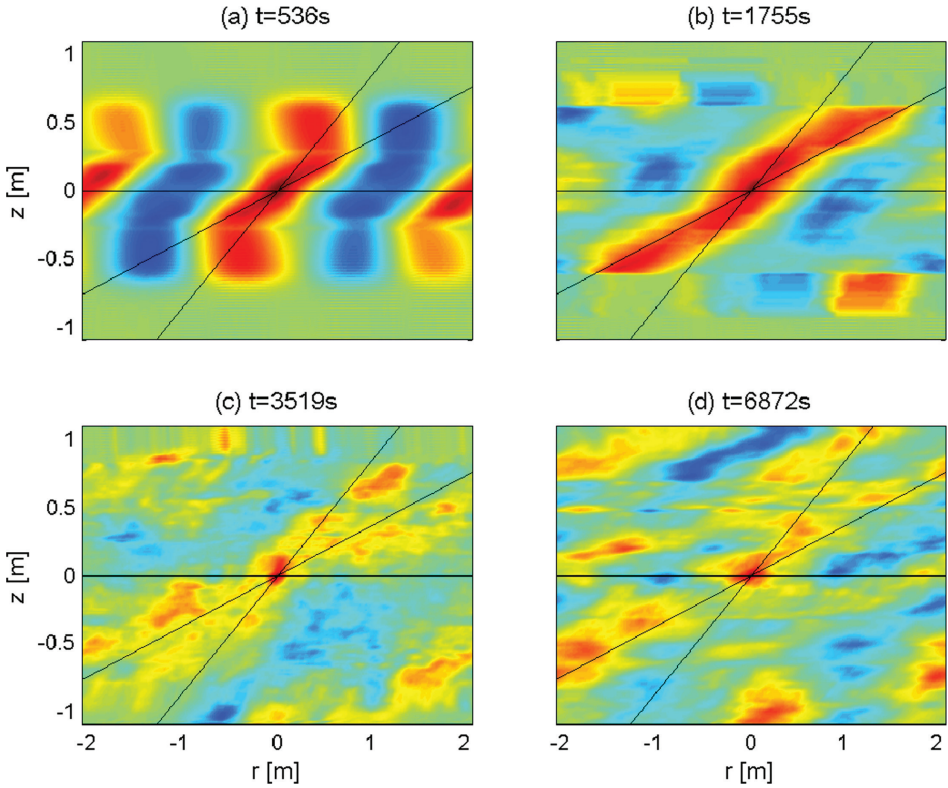
Figure 2. Density autocorrelation function $C_{\rho\rho}$ at $t = 536s$ (a), $t = 1755s$ (b), $t = 3519s$ (c) and $t = 6872s$ (d). The flow is sampled at $y = 0$ and correlations are referenced to $z_0 = 0$. Values range from -1 (blue) to $+1$ (red). Black lines indicate angles $0°$, $20°$ and $40°$.

To place the present results in this wider context, we use the autocorrelation function of the density field, computed as

$$C_{\rho\rho}(r, y, z_0, z, t) = \frac{\langle \rho(x - r, y, z_0, t)\rho(x, y, z, t)\rangle}{\langle \rho(x, y, z_0, t)^2\rho(x, y, z, t)^2\rangle^{1/2}}, \qquad (2)$$

where the angle bracket indicates an average over x. For the examples shown in Figure 2, correlations are taken with respect to the central plane $z_0 = 0$, and the cross-stream coordinate is fixed at $y = 0$.

The general tilt of the isocorrelation contours is in the direction of the mean shear, consistent with previous lab studies (e.g. Tavoularis and Corrsin, 1981; Keller and Van Atta, 2000) and observations in the surface mixed layer of a lake (Ozen *et al.*, 2006). This tilt is consistent with perturbation streamlines tilted *against* the shear, showing a transfer of kinetic energy from the mean flow. Late in the linear growth phase, two wavelengths of

the primary instability are visible (Fig. 2a). Outside the range of the billow heights, the correlation contours are vertical and represent vertically evanescent gravity waves. During the pairing phase (Fig. 2b), the tilted disturbance shows only a single dominant wavelength and covers an expanded vertical region, while the two wavelengths of the primary instability remain evident in the evanescent disturbances near the upper and lower boundaries. After the transition to turbulence (Fig. 2c,d) the correlation function becomes much more complex. The detailed distribution depends on the choices of y and z_0, but tilt in the range $20-40°$ remains dominant, suggesting continued extraction of kinetic energy from the mean flow.

b. Profiler estimates of the displacement scale

To simulate the results of a profiler[3] measurement, density is computed on straight lines (transects) that traverse the shear layer at various locations, angles and times. Acceleration of the instrument by the flow is neglected.[4] Each transect covers the entire vertical extent of the computational domain. Any transect that leaves the domain through a lateral side re-enters through the opposite side, consistent with the periodic boundary conditions. The point where each trajectory intersects the plane $z = 0$ is denoted $\{x_0, y_0\}$. The transect direction is defined by angles of elevation α and azimuth ϕ, both of which are measured from the positive x direction.

Each density profile is reordered as in Thorpe (1977) to produce the vertical displacement $\delta(z)$ and its root-mean-square (RMS) average, the displacement scale (or Thorpe scale) $L_T(x_0, y_0, \alpha, \phi, t)$.[5] The latter applies to a single, linear transect through a flow volume. An additional RMS average is then taken over $-L_x/2 < x_0 < L_x/2$ and $-L_y/2 < y_0 < L_y/2$ to give $\langle L_T \rangle(\alpha, \phi, t)$, which pertains to the entire volume.

In the DNS example described in Section 2a, the RMS displacement scale from vertical profiles $\langle L_T \rangle(90°, 0, t)$ rises to a maximum as the billows pair, then decays (Fig. 3, solid curve). Superimposed on this pattern is a weaker, oscillatory behavior corresponding to the periodic exchange between kinetic and potential energy (Klaassen and Peltier, 1985). The growth and decay of the KH billow has been explored in numerous studies and was validated against microstructure observations in Smyth *et al.* (2001).

The salient point to note in Figure 3 is the difference between results from vertical profiles (solid curve) and transects taken at $\alpha = +30°$ (dotted) and $-30°$ (dashed). To begin with, the oscillation noted above is phase-shifted relative to the vertical profiles. The clearest

---

3. In our terminology "gliders" are a subset of "profilers." Gliders generally move diagonally, while "profilers" also includes instruments designed either for vertical or horizontal motion.

4. This is justified provided that the instrument moves rapidly with respect to current fluctuations. In the case discussed here, the net velocity difference across the shear layer (which approximates the maximum velocity fluctuation) is 0.01 m/s, so a glider traveling O(0.1 m/s) or faster should maintain a straight path. This requirement is likely to be more stringent in strongly sheared oceanic flows.

5. Consistent with observational practice (Moum, 1996; Smyth *et al.*, 2001), the RMS average is taken over a layer bounded above and below by the first and last points at which δ is nonzero. Any subrange of z thicker than 0.1 m in which $\delta = 0$ is excluded from the average. Examples are shown in Figures 6 and 7, right-hand frames.
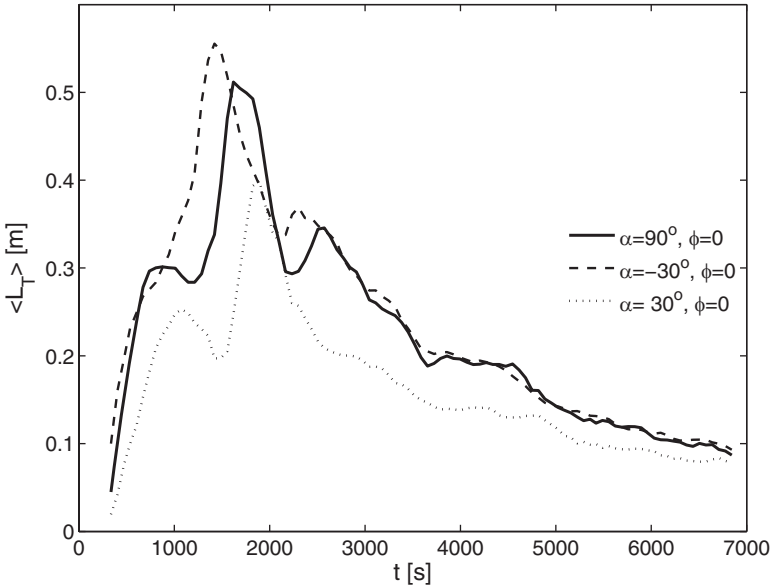
Figure 3. Displacement scale $\langle L_T \rangle (\alpha, 0, t)$ for the mixing event shown in Figure 1. $\langle L_T \rangle$ is computed from 160 streamwise transects crossing a regular grid of (x_0, y_0) values. Elevation angles α are $90°$ and $\pm 30°$ as indicated in the legend.

example is the global maximum in $\langle L_T \rangle$, which is evident at $t = 1400s$ in the transects taken at $\alpha = -30°$ (leaning against the shear), then appears near $t = 1600s$ in the vertical profiles and at $t = 1800s$ for $\alpha = +30°$. The same phase shift is evident between vertical and $30°$ in the earlier peak, and between $-30°$ and vertical in the later peak. Secondly, the transects at negative angles are biased towards higher $\langle L_T \rangle$, while those at positive angles consistently underestimate $\langle L_T \rangle$.

These differences have important implications for profiling at nonvertical angles. Estimates of $\langle L_T \rangle$ could be off by tens of percent. Estimates of the dissipation rate (obtained by assuming that the Ozmidov scale equals the displacement scale, e.g. Dillon (1982)) are proportional to $\langle L_T \rangle^2$, and could therefore have relative errors twice as large. The bias in $\langle L_T \rangle$ due to trajectory angle is characterized by the ratio

$$Bf(\alpha, \phi, t) = \frac{\langle L_T \rangle (\alpha, \phi, t)}{\langle L_T \rangle (90°, 0, t)}. \tag{3}$$

The denominator is the RMS displacement scale for an ensemble of vertical profiles. This ratio gives an estimate of the bias in the displacement scale that would result if many instantaneous profiles were made through the shear layer in a given direction α, ϕ and at a given stage in the evolution of a mixing event.
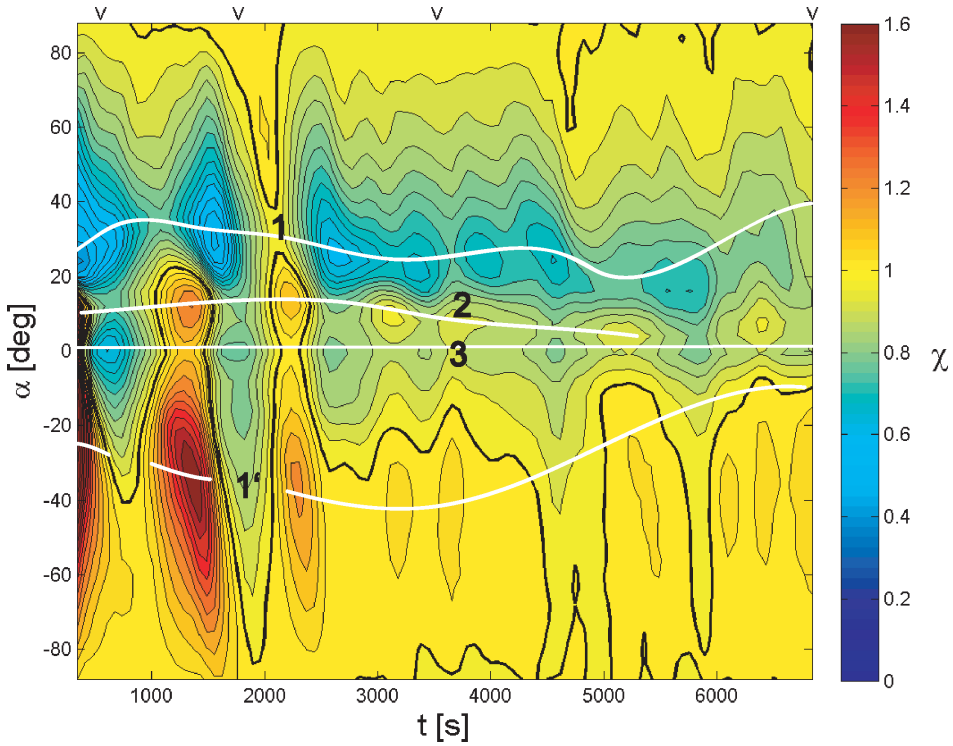
Figure 4. Bias function $Bf(\alpha, 0, t)$ derived from DNS. Thick contour indicates $Bf = 1$. Numbered curves indicate features discussed in the text. Carets at the upper edge indicate times shown in Figures 1 and 2.

3. Results

a. General features of the bias function in a simulated KH billow

The bias function Bf is now examined using the definition (3), with $\phi = 0$, and the DNS model (Section 2a) of the KH billow to determine $\langle L_T \rangle$. The time dependence of the bias function is complex (Fig. 4), but there are two main types of variation that we can identify. The first is a quasiperiodic oscillation on a time scale of 500–1000s. This is due to the rotation of the KH vortex by the background shear, as discussed in Section 2b. The second is the slower variation as the billows break down into stratified turbulence. The latter will be our main focus here.

Throughout this time evolution, the α-dependence of the bias function exhibits several consistent features (highlighted in Figure 4 by white curves).

1. The bias function is approximately asymmetric with respect to α. At sufficiently positive α, there is a tendency toward $Bf < 1$ (blue-green). The smallest Bf values

lie approximately along the curve marked 1. In contrast, Bf tends to be greater than 1 at sufficiently negative α, with maxima lying on the curve 1′. The boundary between these regimes, i.e. the contour $Bf = 1$, oscillates strongly, especially in the first few thousand seconds (the preturbulent regime) then relaxes to a value around $-20°$.

2. A secondary local maximum appears at small positive angles (marked 2). This peak is highly intermittent, but it is at all times a local maximum with respect to α.

3. While there is a minimum at $\alpha = 0$ (marked 3), Bf does not reach as low as zero, the value for a single elliptical vortex (T12).

b. The transition to turbulence

As is inevitable in numerical simulations (as well as lab experiments and *in situ* observations), the present results pertain only to a single example of the wide range of flow geometries attainable in nature. How, then, are we to assess their general relevance? One way to address this problem is to tie the results to clearly identifiable physical phenomena which are known to occur over a significant range of parameter space. In this section we show how the evolution of the bias function can be understood in terms of the properties of KH billows and the turbulence that results.

i. Preturbulent billows We will look first at the laminar KH billow just before pairing, exemplified by the case shown in Figure 1a. The corresponding bias function (Fig. 4 at $t = 536$ s, marked by the first caret at the upper edge of the frame) is shown in Figure 5. At this stage the billows (Fig. 1a) are approximately elliptical with tilt angle $\beta = -20°$ (i.e. the major axis is tilted clockwise from the x direction) and aspect ratio 0.43. The thin curves on Figure 4 show $Bf(\alpha)$ derived from Eq. (9) of T12 using these parameter values. Dashed segments indicate trajectories that would intersect neighboring billows, assuming periodic ellipses with spacing equal to twice the major axis, as is approximately true in Figure 1a. We now seek to explain the features labeled 1, 1', 2 and 3, all of which differ to some degree from the simpler model of T12.

The asymmetry between positive and negative α, whose extremes are marked 1' and 1, is also evident in the elliptical vortex model, though to a lesser degree. In that model, the asymmetry requires that $\beta < 0$.[6] As noted in Section 2a, $\beta < 0$ is consistent with the growth of the KH instability via extraction of kinetic energy from the mean shear. The asymmetry in Bf is also due in part to the spiral structure of the density field, a property not considered in T12. To see the effect on feature 1', compare the transect at negative $\alpha = -40°$ (Fig. 6b) with that at $\alpha = 90°$ (Fig. 6a). For definiteness, focus on the upper half of the billow. The transect at $\alpha = -40°$ encounters fluid in about the same vertical range as the vertical transect (as in the elliptical vortex model), but the fluid it encounters is denser (center panels), i.e. it has been lifted further from its equilibrium height. This is shown more clearly in the middle

6. More precisely, in (9) of T12, $Bf < 1$ for α slightly less than 90° (and $Bf > 1$ for α slightly greater than $-90°$), provided that $\beta < 0$. The opposite asymmetry holds if $\beta > 0$.
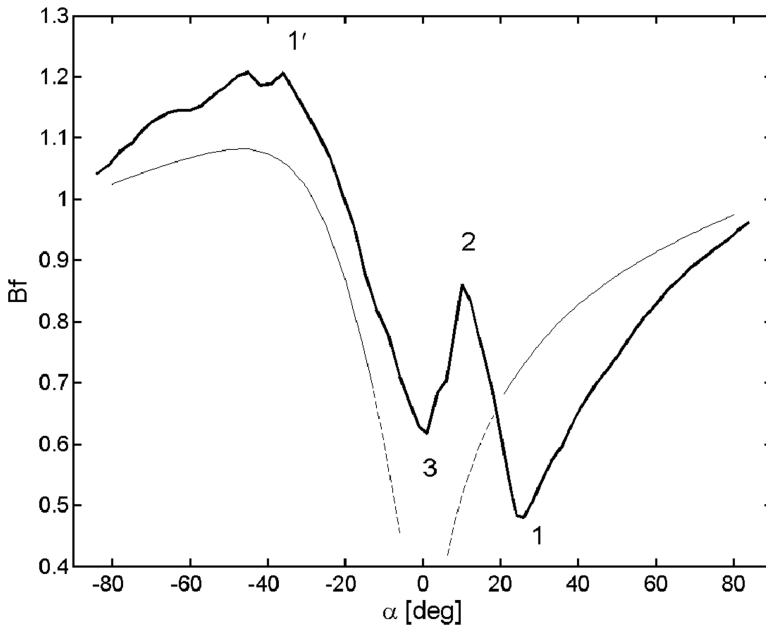
Figure 5. Solid: Bias function $Bf(\alpha, 0, 536\,s)$ from the DNS model, corresponding to the first caret at the upper edge of Figure 4. Thin curve: Bias function for the elliptical vortex model of T12. In dashed sections, trajectories encounter more than one billow. Numerical labels indicate points discussed in the text.

panel of (b), where density profiles at $\alpha = -40°$ (thick solid) and $\alpha = 90°$ (thin solid) are overlaid for comparison. As a result, the extent of the displacements (right panel) in the sloping transect exceeds those in the vertical transect (vertical lines), and the resulting RMS value is larger by about 11%. In contrast, the transect at $\alpha = 40°$ (Fig. 6c) gives an underestimate of $\langle L_T \rangle$ (marked "1" on Fig. 5; also see white curve on Fig. 4) because it does not encounter displaced fluid until after it has passed its maximum displacement.

Any horizontal vortex in a stably stratified fluid advects isopycnals into a spiral pattern like that shown in Figure 6, and the effect of vortex tilt ($\beta < 0$) adds to the resulting asymmetry. The tendency for $\langle L_T \rangle$ to be overestimated (underestimated) from a transect tilted against (with) the vorticity should therefore be a common property of such vortices. An exception can occur if a billow is in the process of collapsing such that some of its kinetic energy is returned to the mean flow, in which case the effective value of β is positive. The effect of $\beta > 0$ can then balance that of the spiral density structure. An example is visible on Figure 4 between $t = 1900\,s$ and $t = 2100\,s$, at which point the billow is collapsing (Fig. 3) and Bf is near unity for all α. We emphasize that this interval is brief, and that the asymmetry in Bf discussed above is almost always present.

Feature 2, the sharp peak in Bf at $\alpha \approx 10°$, is due to false overturns registered when the profile crosses the braid at a low angle and intersects the two adjoining billows (Fig. 7a).
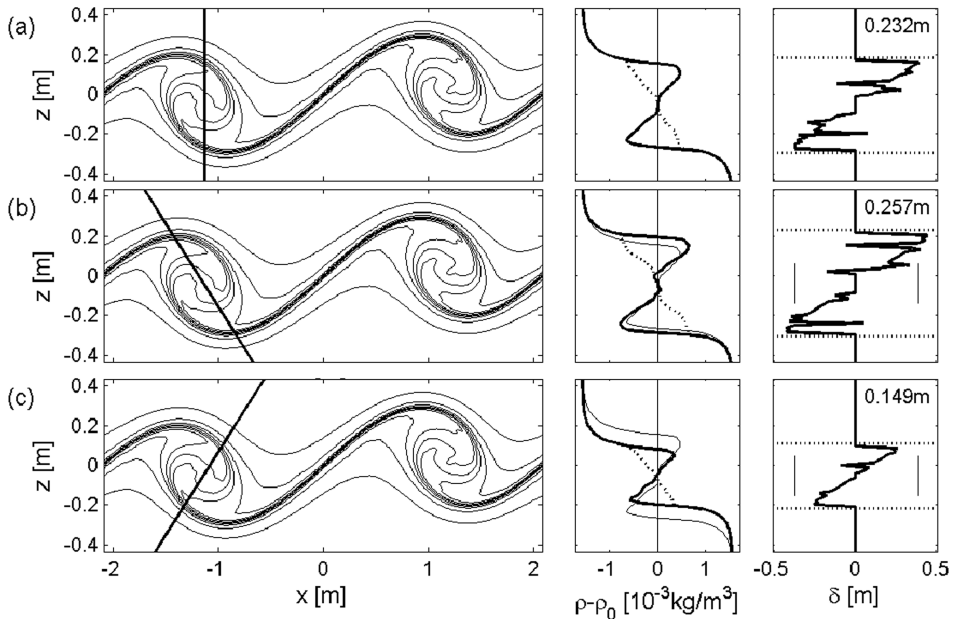
Figure 6. Left panels: Isopycnals showing the geometry of KH billows just as pairing begins. Lines indicate transects taken through the billow core at $\alpha = 90°$ (a), $\alpha = -40°$ (b), and $\alpha = +40°$ (c). The intercept x_0 is chosen so that the transect intersects the braid core. In all cases $y_0 = 0$. Center panel: Density profiles through the transects shown at left. Dotted curves show reordered density. In (b) and (c), the density profile from (a) is reproduced as a thin curve. Right panels: Vertical displacement $\delta(z)$. Annotations show the RMS displacement L_T. In (b) and (c), vertical lines show the extremes of δ in the vertical case (a). Horizontal dotted lines show the boundaries over which the RMS averages are taken to define L_T.

The RMS displacement scale 0.213 m is within 8% of the vertical profile value, despite the fact that the profile encounters overturned fluid only in small regions near the top and bottom of the billows. A similar effect is found when the braid is crossed at a small negative angle (Fig. 7b). The profile intersects the upper part of the left billow and the lower part of the right billow, in each case producing the appearance of an overturn although, in this case, the sampled fluid is stable throughout. Here the measured displacement scale is only 0.110 m. It is therefore not surprising that Figure 5 shows no corresponding peak in Bf at small negative α.

The measured density profile in Figure 7 suggests two smaller overturns separated by a sharp layer of stable stratification, a fact which could further confuse the interpretation. The RMS average displacement, however, is the same whether the "overturns" are counted as one event or two.

The fact that Bf is greater than predicted at very low angles (e.g., feature 3 on Fig. 5) is accounted for by the fact that the elliptical vortex model describes only a single billow, while
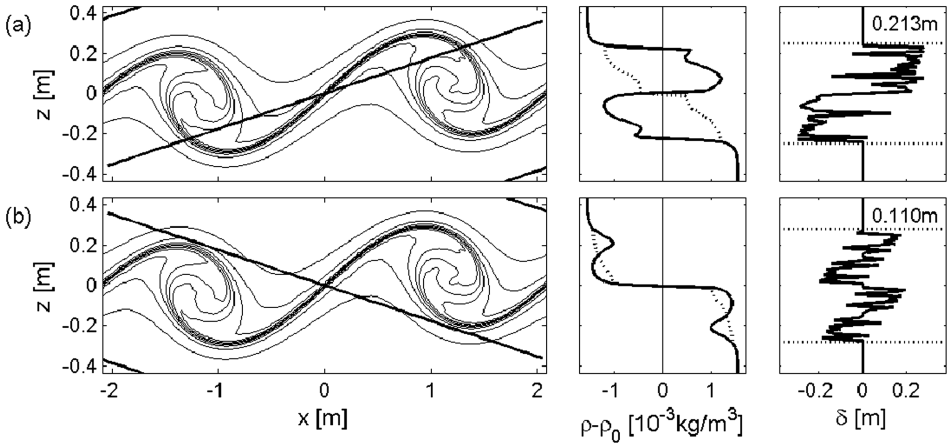
Figure 7. Left panels: Isopycnals showing the geometry of KH billows just as pairing begins. Lines indicate transects taken through the braid at $\alpha = 10°$ (a) and $\alpha = -10°$ (b). Center panel: Density profiles through the transects shown at left. Dotted curves show reordered density. Right panels: Vertical displacement $\delta(z)$. Annotations show the RMS displacement L_T. Horizontal dotted lines show the boundaries over which the RMS averages are taken to define L_T.

DNS represents a periodic billow train. Low-angle transects therefore encounter multiple billows, which contain displaced fluid over most of the vertical range of the billow train. In the limit $\alpha \to 0$, the streamwise distance covered by the transect goes to infinity, and the measured displacement scale asymptotes to a nonzero limit. This limit would represent an upper bound in the real ocean, where billows trains typically comprise $\sim O(10)$ billows (e.g. Moum *et al.*, 2011). The elliptical vortex model predicts $Bf = 0$ for a single billow, likely to be pertinent for short billow trains, and $Bf = \sqrt{3/2}$ for the limit of an infinitely long billow train (T12). The present value is influenced by the fact that pairing has already begun at $t = 536$ s, so that a transect at very small α can yield false overturning.

In summary, the differences from T12 shown in Figure 5 are due to the facts that (a) the simulated preturbulent billows have spiral density structure which influences $\langle L_T \rangle$ (though not the billow height as computed in T12) and (b), the simulations assume an infinite train of billows as opposed to the single-billow limit of T12.

ii. Turbulence Perhaps the most remarkable aspect of the bias function in the turbulent stage is its overall similarity to the laminar stage, despite the fact that the KH billows have broken down (Fig. 8, compare with Fig. 5). While Bf is generally closer to unity, the higher bias at negative α, the peak at $\alpha \sim 10°$ and the lower bias at steeper positive angles are still visible.

An accumulation of evidence suggests that stratified, sheared turbulence can produce flow features reminiscent of KH billows (with braid-core structure and negative tilt), a circumstance that would account for the persistent asymmetry of the bias function. For
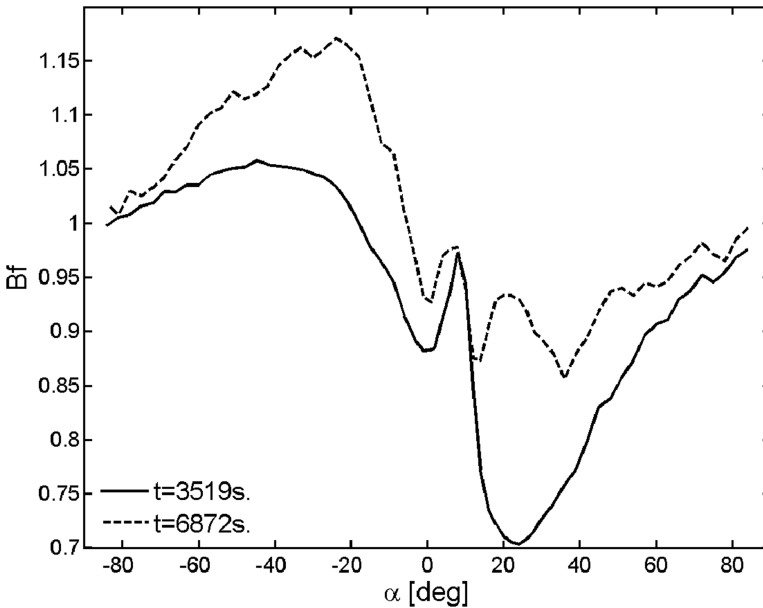
Figure 8. Bias functions $Bf(\alpha, 0, 3519\,s)$ and $Bf(\alpha, 0, 6872\,s)$, corresponding to the third and fourth carets at the upper edge of Figure 4.

example, a sequence of observational studies has revealed a persistent skewness of $-0.75\pm$ 0.25 in the distribution of the streamwise temperature derivative in naturally occurring turbulent shear flows (e.g., Thorpe and Hall, 1980; Thorpe, 1985). DNS has revealed a similar skewness value in turbulence arising from KH billows (Smyth and Moum, 2000b). In another DNS study, Smyth (1999) showed that, in a volume average over turbulence resulting from breaking KH billows, the middle eigenvalue of the strain tensor is positive. This indicates that, over most of the volume, flow features are compressed in one direction and stretched in the other two, leading to the "pancake" geometry of which the KH braids are an example. In about one quarter of the volume, however, the middle eigenvalue is negative, indicating the creation of one-dimensional vortex structures such as the KH cores.

In the present DNS, comparison of the autocorrelation function in the early and late turbulent phases (Figs. 2c and d, respectively) suggests a change in flow structure. In the former, the gravest horizontal wavelength is still visibly dominant, likely a remnant of the paired KH billow. In contrast, the late turbulent phase shows strong correlations at shorter wavelengths more like the primary KH instability. Correlation maxima are not focussed near $z = 0$ as in the linear regime (Fig. 2a), but rather are spread irregularly throughout the volume.

The skewness of the density gradient (S_ρ, opposite in sign to that of the temperature gradient) remains positive throughout (Fig. 9), consistent with the observations cited above of ramplike structures in sheared turbulence. In the preturbulent and pairing phases, the
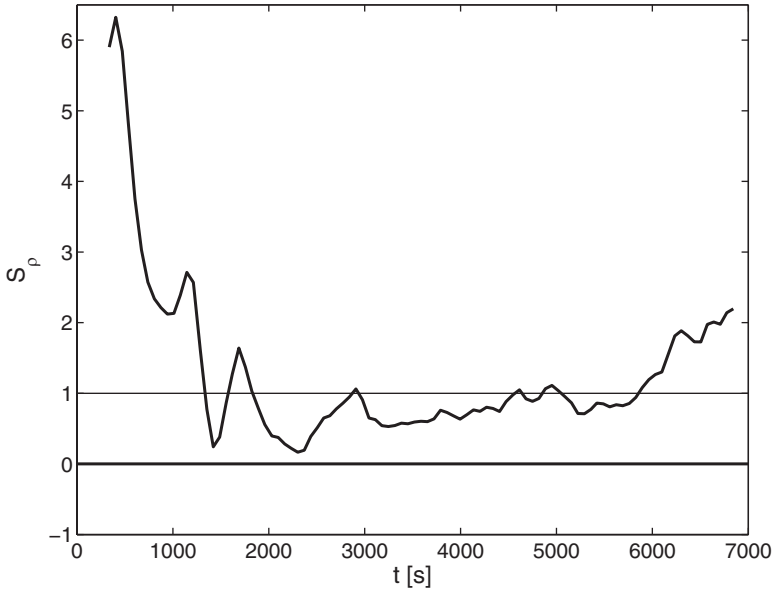
Figure 9. Skewness of the density field S_ρ. Positive values indicate that the mean is dominated by a
    few large (positive) values.

skewness is highly variable and generally large. In the turbulent phase, the skewness settles
down to a value near unity, quantitatively consistent with the observations referenced above.
During the final 1000 s of the run, S_ρ increases markedly, attaining values around 2.

Changes in both the autocorrelation and the skewness of the density gradient in the late
stage of the simulation suggest re-emergence of KH billows, on the scale of the primary
instability or smaller. These are evident in Figure 1d, and may be caused by concentrations
of shear due to interactions between larger-scale flow structures. (The latter could be gravity
waves or remnant vortices from a previous flow stage. A simple example is the secondary
billows shown in Fig. 1b.) Emergence of coherent billows in the turbulent decay stage is also
evident in the previous DNS of Smyth and Moum (2000a) (their Figs. 8a, 9a) and in the lab
experiments of Keller and Van Atta (2000). Because these late structures have the familiar
geometry of KH billow trains (braids separating spiral cores), it is not surprising that the
essential structure of the bias function ($Bf > 1$ at steep negative α, the peak at $\alpha \sim 10°$,
$Bf < 1$ at positive α, as shown in Fig. 8) remains unchanged.

c. Effects of horizontal intermittency

We next examine the variability of the displacement scale as a function of (x_0, y_0), the
point where the transect intersects the plane $z = 0$. For each α, 640 transects were made
on a regular grid in $\{x_0, y_0\}$, and the mean, median and quartiles of L_T were computed
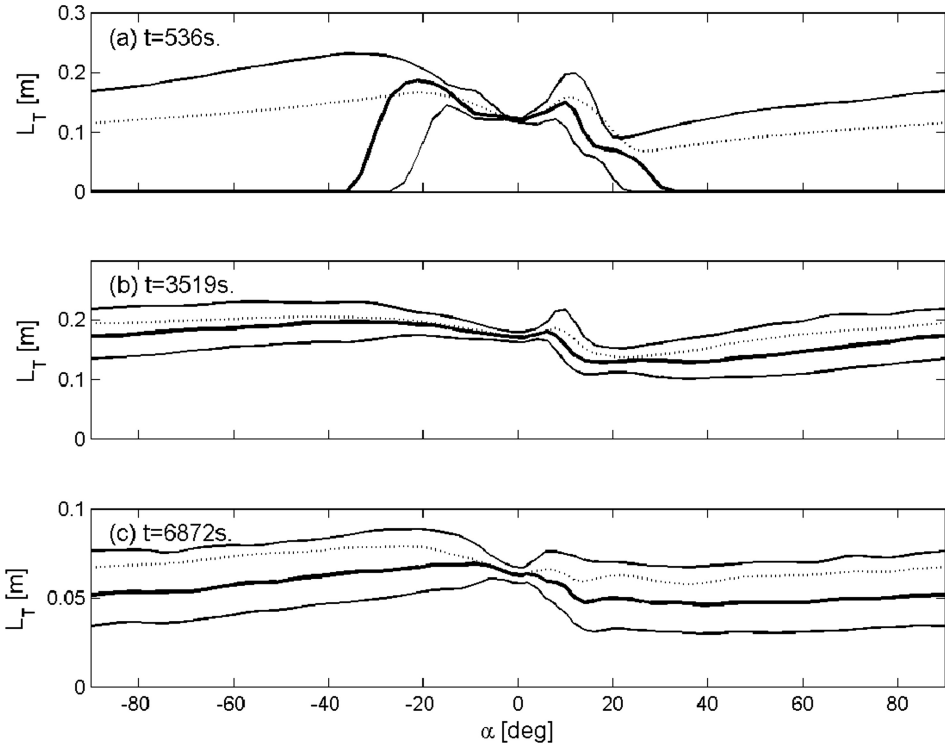(Fig. 10).

Figure 10. Statistics of the RMS displacement scale L_T as a function of α. Solid curves denote the median (thick) and the upper and lower quartiles (thin). The dotted curve represents the RMS mean. Computations were done at $t = 536$ s (a), $t = 3519$ s (b) and $t = 6872$ s (c).

Statistics in the preturbulent case (Fig. 10a) are easily understood as a result of the clear separation between the braids and cores of the KH billow train. For α approaching $\pm 90°$ (nearly vertical), the majority of profiles do not intersect a core, and hence register no over-turning. Because of this, the median value of L_T (thick curve, near left and right edges of Fig. 10a) is zero. Some of these near-vertical profiles do intersect overturned regions, how-ever, so that the upper quartile (upper thin curve) and the mean (dotted curve) are nonzero.

The probability of encountering a billow core increases for profiles that tilt away from the vertical. In the range $-35° < \alpha < 30°$, more than half of the profiles register overturning, so that the median of L_T becomes nonzero. In the range $-25° < \alpha < 20°$ this is true of three quarters of profiles, so that the lower quartile becomes nonzero.

As profiles approach the horizontal ($\alpha \approx 0$), they encounter multiple billows and therefore record increasingly similar samplings of overturned fluid. In the horizontal limit $\alpha \to 0$, the mean, the median, and the upper and lower quartiles converge to a single value. This convergence reflects the general irrelevance of x_0 for horizontal profiles. This particular result is also independent of y_0, since the flow in the preturbulent stage does not vary with y.

In the turbulent cases (Figs. 10b and c), the overturned regions are distributed quasi-randomly throughout the fluid, so the dependence on α is considerably reduced. As in the preturbulent phase, the range of values constricts near $\alpha = 0$, though it does not vanish as in Figure 10a because the flow now depends on y.

d. Dependence on ϕ

Here we present a brief investigation of profiles with nonzero ϕ. The present DNS is not optimal for this aspect of the study, as the computational domain does not accommodate the spanwise scales needed for the knot instabilities that are frequently observed in the later stages of KH evolution (Thorpe, 2002) and which influence the spanwise coherence length of the billows. [The domain was designed to accommodate four wavelengths of the secondary instability that introduces shear-aligned convection rolls in the cores (Klaassen and Peltier, 1991).]

For the two-dimensional elliptical vortex (T12), when $\phi = \pm 90°$, the density profile recorded at any elevation angle α (other than zero) is indistinguishable from the corresponding vertical profile. As a result, $Bf \rightarrow 1$ in the limit $\phi \rightarrow \pm 90°$. The same is true for the pre-turbulent stage of the simulated KH billows, as they are likewise independent of y (Fig. 11a). For $\phi \neq \pm 90°$, Bf can depart from 1. The extremum of Bf is not necessarily at $\phi = 0$.

With the appearance of three-dimensional instabilites (Klaassen and Peltier, 1991), it is no longer necessary that $Bf \rightarrow 1$ when $\phi \rightarrow \pm 90°$. This is approximately true, though (Fig. 11b,c), and the greatest biases generally occur for ϕ other than $\pm 90°$. By symmetry, $Bf(-\alpha, \pm 90°, t) = Bf(\alpha, \pm 90°, t)$ as is evident on close inspection of Figure 11c.

4. Implications for observations

a. Choice of trajectory angle

For observational planning, it would be useful to identify the "optimal" direction for transects across a volume in which billows are presumed to exist. The answer depends largely on the spatial distribution of billow patches, which is unknown *a priori*. The present results suggest that high values of ϕ (close to 90°) are advantageous in that they lead to $Bf \approx 1$ (Fig. 11). Inevitably, and possibly by design, ϕ may be other than 90°, in which case the dependence on α becomes important.

A testable prediction based on time-averaged Bf (Fig. 12) is that, for streamwise profiles ($\phi = 0$), $\langle L_T \rangle$ should be relatively large when $\alpha < \alpha_1$, where α_1 is a small negative angle. Conversely, $\langle L_T \rangle$ should be relatively small when $\alpha > \alpha_1$. The exact value of α_1 may be sensitive to the details of the initial flow; for the present case $\alpha_1 = -15°$. The maximum high bias is about 1.10 and occurs at $\alpha = -40°$, while the minimum bias is 0.75 at $\alpha = 25°$. The difference between $\langle L_T \rangle$ at $\alpha > \alpha_1$ and $\alpha < \alpha_1$ can therefore be as great as $\sim 40\%$.[7]

---

7. Recall that the degree of bias at low $|\alpha|$ depends on the length of the billow train, which is infinite in our DNS (due to the periodic boundary conditions) but finite in naturally occurring flows.
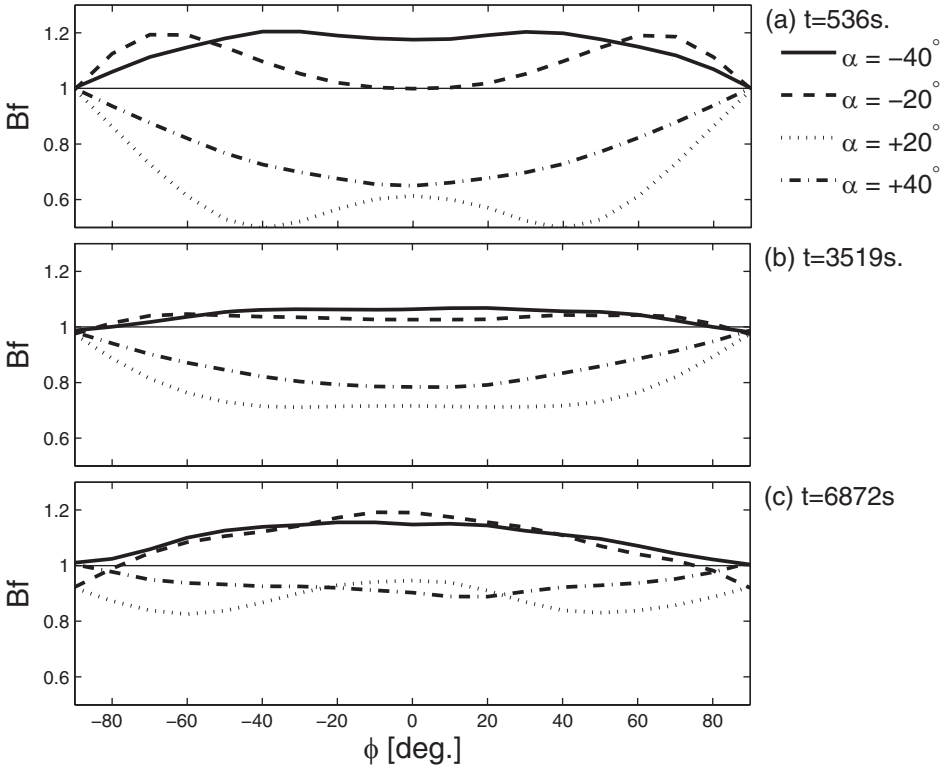
Figure 11. Bias function versus the azimuthal angle ϕ for preturbulent (a), early turbulent (b) and late turbulent (c) stages and various α as shown in the legend.

b. Practical convergence criteria

For the most part, the displacement scales and other turbulence statistics discussed so far have been based on ensembles of many profiles taken through the same turbulent event at the same time. At present this is impossible in the field; instead, it is common that a mixing event is represented by at best a single profile. In that case, results from Section 3d tell us that the displacement scale deduced from a single vertical profile through billows in the early turbulent phase has a 50% likelihood of falling within ~25% of the median (see Fig. 11b, in particular the spread of the quartiles at $\alpha = \pm 90°$). By this measure, intermittency is greater in both the preturbulent (Fig. 11a) and late turbulent (Fig. 11c) phases.

We may reasonably hope that new observational technologies will allow multiple simultaneous profiles (Thorpe, 2011). Even where simultaneous profiles are not possible, it might be assumed that the flow field in a given region includes many similar mixing events. In this case a large ensemble of profiles is to some extent equivalent to many profiles through the same event, and statistical averages can be meaningfully associated with a "typical" event
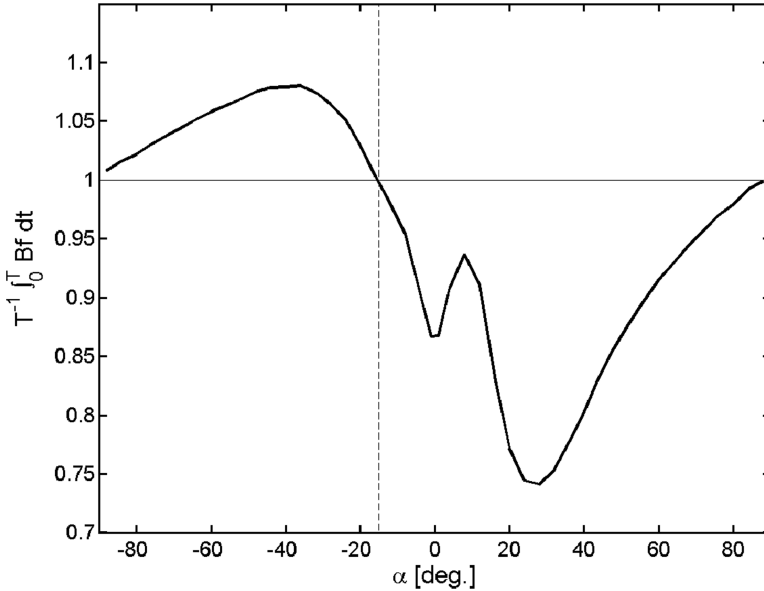
Figure 12. Time-averaged bias function $T^{-1} \int_0^T Bf(\alpha, 0, t)dt$, where $T = 6872s$, for the billows illustrated in Figure 1. The vertical dashed line indicates $\alpha_1 = -15°$, the "optimal" angle for a streamwise profile. This value is sensitive to parameter choices.

(Moum *et al.*, 2011; Smyth *et al.*, 2011). It would therefore be useful to extend the results of Section 3d by determining the number of profiles through a single event (or, equivalently, through many statistically similar events) that would be needed to estimate the displacement scale with a prescribed level of accuracy. For example, this will allow estimation of the number of event encounters needed to test the predicted α-dependence of Bf.

We have estimated $\langle L_T \rangle$ by averaging results from many (10^4) randomly-chosen sets of M profiles at different horizontal locations (x_0, y_0). Here we discuss three representative examples drawn from the preturbulent, early turbulent and late phases of the simulation, in which the profiles were vertical. (We have seen that intermittency is greatest for vertical profiles.) In contrast to Section 3d, profiles yielding $L_T = 0$ were omitted from these statistics, as they would be in the analysis of observational data.

Consider first the preturbulent case. A single profile has an 81% chance of giving the RMS average $\langle L_T \rangle$ to within 40%, as may be seen by examining Figure 13a, solid curve, left-hand edge. The probabilities that a single measurement will be within 20% and 10% of the RMS average are 53% and 22%, respectively (dashed and dotted curves). As the number of profiles increases, so does the probability of attaining any specified level of accuracy. If 6 profiles are available, one is virtually certain (at the 95% confidence level) to estimate $\langle L_T \rangle$ to within 20%. With 20 profiles, the estimate should be correct to within 10%. For non-vertical profiles, this source of uncertainty is generally smaller (Section 3d). To detect
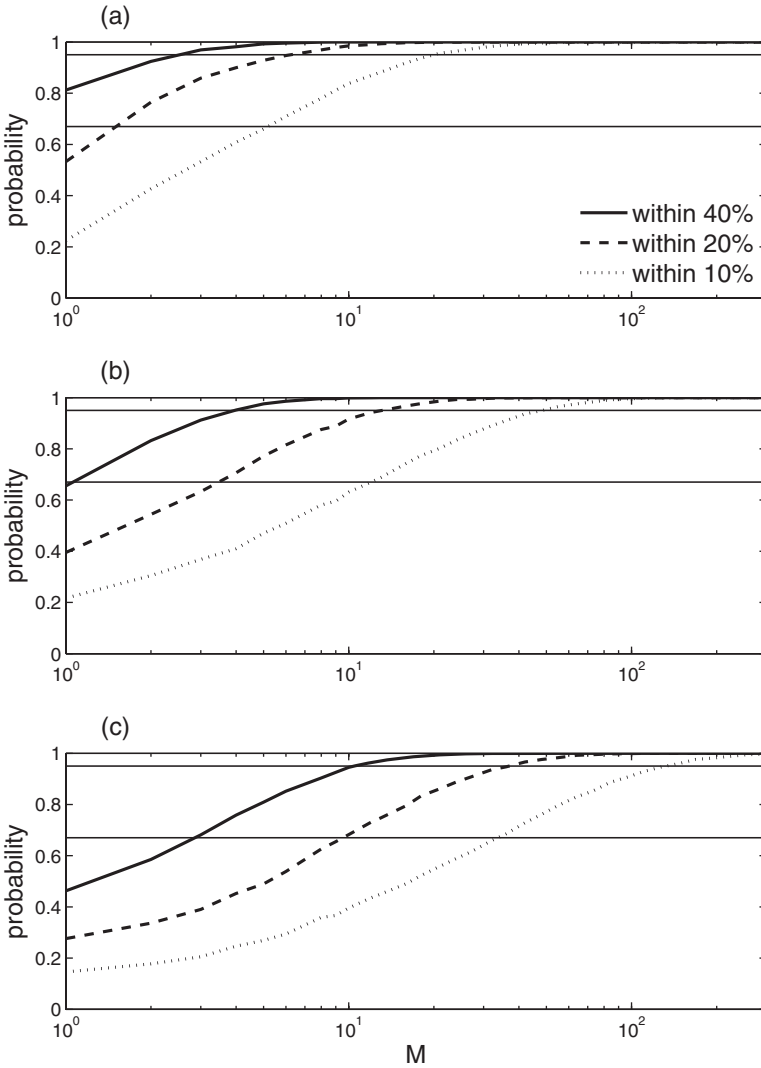
Figure 13. Probability that the root mean square of L_T will be measured to a given degree of accuracy by the average of M profiles. Horizontal lines indicate confidence levels of 67% and 95%.

the predicted difference between positive and negative α (Section 4a), the uncertainty in $\langle L_T \rangle$ must at least be less than the maximum difference, 40%. To conduct this test with confidence, one might reasonably judge that an uncertainty of 10% is acceptable, in which case at least 20 event encounters would be needed.

As the flow evolves, accurate estimation of $\langle L_T \rangle$ requires a denser ensemble of profiles. In the early turbulent stage (Fig. 13b), 50 profiles are needed to be certain (at the 95%

confidence level) of estimating $\langle L_T \rangle$ to within 10%. By the late turbulent phase, 10% accuracy requires about 130 profiles. These estimates can be relaxed, of course, if one is willing to accept a lower confidence level, such as 67% as shown by the lower horizontal lines.

If the displacement scale is being used to estimate the dissipation rate ϵ via the Ozmidov scale (e.g., Dillon, 1982), the uncertainty in ϵ is proportional to the square of the uncertainty in $\langle L_T \rangle$. The probabilities quoted above for estimating $\langle L_T \rangle$ to within 10%, 20% and 40% therefore apply to the probability of estimating ϵ to within approximately 20%, 40% and a factor of 2, respectively. We must keep in mind that the numerical values given above, while probably typical, depend on parameter choices (e.g. the Richardson and Reynolds numbers of the initial flow) as well as the angle ϕ and the evolutionary stage of the billows.

c. A proposed experiment

The use of automated gliders operating at angles of a few tens of degrees from the horizontal promises to deliver far greater numbers of event encounters than has been possible using locally-attended profilers. The present results suggest that bias due to trajectory tilt is not an insurmountable obstacle, and may even be useful in diagnosing the mechanism of mixing. Suppose that a glider makes many transects in a region of steady, parallel shear (so that billow orientation can be guessed *a priori*), such as the upper flank of the Pacific Equatorial Undercurrent (EUC). Suppose also that the transects follow a tow-yo pattern with horizontal component in the direction of the mean shear (which is generally zonal) and alternating positive and negative α. The glider would encounter a large number of mixing events (Moum *et al.*, 2011; Smyth *et al.*, 2011). With $O(100)$ or more encounters, it should be possible to detect the difference in L_T between events crossed at positive and negative α. It would also be straightforward, based on calculations such as those shown in Figure 12, to select a combination of α values whose resulting Bf's would combine to give unity, and hence an unbiased estimate of $\langle L_T \rangle$. In addition, it would be of interest to compare these estimates with profiles taken at $\phi = 90°$ (the direction of the mean vorticity vector) for which Bf should be close to unity.

5. Conclusions

We have used a DNS model to estimate the effects of tilt angle on the statistics of the displacement scale that would be measured by a glider crossing a train of KH billows. Several compromises have been made that could be mitigated in future studies. The simulated shear flow is started impulsively with a subcritical Richardson number, rather than being continuously depressed to unstable values (Inoue and Smyth, 2009), as occurs in nature. Periodic boundary conditions in x and y imply an infinite train of infinitely wide billows. The Reynolds number is small for the ocean, and artificial upper and lower boundaries prevent us from simulating the entire decay phase. The instrument is assumed to travel in a straight line (i.e. accelerations due to the sheared current are neglected), and rapidly enough

that the billows can be regarded as stationary. With these caveats in mind, we reach the following conclusions.

- Displacement scale estimates can vary by several tens of percent as the tilt angles α and φ are varied.
- Three major biases with respect to α result from the "core and braid" geometry of KH billow trains.
    1. The asymmetry between high Bf at α < 0 and low Bf at α > 0 is due in part to the tilt of the vortex and in part to the spiral structure of density within the cores.
    2. The peak in Bf at small positive α is due to false overturns registered when profiles cross the braids at an angle shallower than the isopycnals.
    3. The nonzero displacement scale at α $= 0$ results fom the periodicity of the simulated billows.

  We therefore suggest that these properties of Bf are common, at least qualitatively, to all billow trains.
- Though pairing and the oscillation of the billow cause momentary changes, the essential structure of the bias function changes little during the transition to turbulence. This suggests that the turbulence itself contains overturning structures similar to KH billows, though on smaller scales and over a range of tilt angles.
- Bias can be reduced by profiling in the cross-stream direction.
- Due to horizontal intermittency, the uncertainty in $\langle L_T \rangle$ in a single profile is likely to be several tens of percent. Insofar as a sheared current may be expected to contain many statistically similar mixing events, this uncertainty may be reduced by averaging results from many profiles. For the applications envisioned here, an ensemble of $O(100)$ profiles through similar events is sufficient to effectively remove the uncertainty.
- Bias in $\langle L_T \rangle$ due to trajectory tilt can provide a useful diagnostic of mixing physics. Alternatively, it can be reduced by averaging over different tilt angles.

Decades of observations have shown that billow trains are common mixing mechanism in strongly sheared oceanic regimes. The workings of individual billows have been studied extensively, but we know little of the spatial and temporal scales of the billow train as a whole and of the processes that determine them. We hope that the present results will help to prepare the way for much-needed further observations of these phenomena.

REFERENCES

Baines, P. and H. Mitsudera. 1994. On the mechanism of shear flow instabilities. J. Fluid Mech., *276*, 327–342.

Dillon, T. 1982. Vertical overturns: a comparison of Thorpe and Ozmidov scales. J. Geophys. Res., *87*, 9601–9613.

—— 1984. The energetics of overturning structures: Implications for the theory of fossil turbulence. J. Phys. Oceanogr., *14*, 541–549.

Eriksen, C. 2009. Gliders. *in* Encyclopedia of Ocean Sciences, 2nd ed., Steele, J., S. Thorpe, and K. Turekian, eds., Elsevier/Academic Press, Boston, 59–66.

Geyer, W., A. Lavery, M. Scully, and J. Trowbridge. 2010. Mixing by shear instability at high Reynolds number. Geophys. Res. Lett., *37*, L22607, doi:10/1029/2010GL045272.

Geyer, W. and J. Smith. 1987. Shear instability in a highly stratified estuary. J. Phys. Oceanogr., *17*, 1668–1679.

Gregg, M. C. 1987. Diapycnal mixing in the thermocline: A review. J. Geophys. Res., *92* (C5), 5249–5286.

Inoue, R. and W. Smyth. 2009. Efficiency of mixing forced by unsteady shear flow. J. Phys. Oceanogr., *39*, 1150–1166.

Keller, K. and C. Van Atta. 2000. An experimental investigation of the vertical temperature structure in homogeneous stratified shear turbulence. J. Fluid Mech., *425*, 1–29.

Klaassen, G. and W. Peltier. 1985. The evolution of finite-amplitude Kelvin-Helmholtz billows in two spatial dimensions. J. Atmos. Sci., *42*, 1321–1339.

—— 1991. The influence of stratification on secondary instability in free shear layers. J. Fluid Mech., *227*, 71–106.

Li, H. and H. Yamazacki. 2001. Observations of a Kelvin-Helmholtz billow in the ocean. J. Oceanogr., *57*, 709–721.

Moum, J. 1996. Efficiency of mixing in the main thermocline. J. Geophys. Res., *101* (C5), 12,057–12,069.

Moum, J., D. Caldwell, J. Nash, and G. Gunderson. 2002. Observations of boundary mixing over the continental slope. J. Phys. Oceanogr., *35*, 2113–2130.

Moum, J., D. Farmer, W. Smyth, L. Armi, and S. Vagle. 2003. Structure and generation of turbulence at interfaces strained by solitary waves propagating shoreward over the continental shelf. J. Phys. Oceanogr., *33*, 2093–2112.

Moum, J., J. Nash, and W. Smyth. 2011. Narrowband, high-frequency oscillations in the upper equatorial ocean: Part 1: Intepretation as shear instabilities. J. Phys. Oceanogr., *41*, 397–411.

Ozen, B., S. Thorpe, U. Lemmin, and T. Osborn. 2006. Cold-water events and dissipation in the mixed layer of a lake. J. Phys. Oceanogr., *36*, 1928–1939.

Seim, H. and M. Gregg. 1994. Detailed observations of a naturally-occurring shear instability. J. Geophys. Res., *99* (C5), 10,049–10,073.

Smyth, W. 2003. Secondary Kelvin-Helmholtz instability in a weakly stratified shear flow. J. Fluid Mech., *497*, 67–98.

—— 2004. Kelvin-Helmholtz billow evolution from a localized source. Q. J. R. Meteorol. Soc., *130*, 2753–2766.

—— 1999. Dissipation range geometry and scalar spectra in sheared, stratified turbulence. J. Fluid Mech., *401*, 209–242.

Smyth, W. and J. Moum. 2000a. Length scales of turbulence in stably stratified mixing layers. Phys. Fluids, *12*, 1327–1342.

—— 2000b. Anisotropy of turbulence in stably stratified mixing layers. Phys. Fluids, *12*, 1343–1362.

Smyth, W., J. Moum, and D. Caldwell. 2001. The efficiency of mixing in turbulent patches: inferences from direct simulations and microstructure observations. J. Phys. Oceanogr., *31*, 1969–1992.

Smyth, W., J. Moum, and J. Nash. 2011. Narrowband, high-frequency oscillations in the upper equatorial ocean: Part 1: Properties of shear instability. J. Phys. Oceanogr., *41*, 412–428.

Smyth, W., J. Nash, and J. Moum. 2005. Differential diffusion in breaking Kelvin-Helmholtz billows. J. Phys. Oceanogr., *35*, 1044–1022.

Tavoularis, S. and S. Corrsin. 1981. Experiments in nearly homogeneous turbulent shear flow with a uniform mean temperature gradient. Part 1. J. Fluid Mech., *104*, 311–347.

Taylor, G. 1931. Effect of variation in density on the stability of superposed streams of fluid. Proc. Roy. Soc. A, *132*, 499–523.

Thorpe, S. 2002. The axial coherence of Kelvin-Helmholtz billows. Q. J. R. Meteorol. Soc., *128*, 1529–1542.

—— 2011. Breaking internal waves and turbulent dissipation. J. Mar. Res., *68*, 851–880.

—— 2012. Measuring overturns with gliders. J. Mar. Res., *70*, 93–117.

—— 1977. Turbulence and mixing in a Scottish loch. Philos. Trans. Roy. Soc. London, *A286*, 125–181.

—— 1978. The near-surface ocean mixing layer in stable heating conditions. J. Geophys. Res., *83*, 1529–1542.

—— 1985. Laboratory observations of secondary structures in Kelvin-Helmholtz billows and consequences for ocean mixing. Geophys. Astrophys. Fluid Dyn., *34*, 175–199.

—— 1987. Transition phenomena and the development of turbulence in stratified fluids. J. Geophys. Res., *92*, 5231–5245.

Thorpe, S. and A. Hall. 1980. The mixing layer of Loch Ness. J. Fluid Mech., *101*, 687–703.

Thorpe, S. and J. Holt. 1995. The effects of laterally sloping upper and lower boundaries on waves and instability in stratified shear flows. J. Fluid Mech., *286*, 49–65.

Van Haren, H. and L. Gostiaux. 2009. High-resolution, open-ocean temperature spectra. J. Geophys. Res., *114*, C05005, doi:10.1029/2008JC004967.

Wijesekera, H. and T. Dillon. 1997. Shannon entropy as an indicator of age for turbulent overturns in the oceanic thermocline. J. Geophys. Res., *102* (C2), 3279–3291.

Winters, K., J. MacKinnon, and B. Mills. 2004. A spectral model for process studies of rotating, density-stratified flows. J. Atmos. Oceanic Technol., *21*, 69–94.

Woods, J. 1968. Wave-induced shear instability in the summer thermocline. J. Fluid Mech., *32*, 791–800.